

## Non-invasive estimation of pulsatile flow and differential pressure in an implantable rotary blood pump for heart failure patients

This article has been downloaded from IOPscience. Please scroll down to see the full text article.

2009 Physiol. Meas. 30 371

(<http://iopscience.iop.org/0967-3334/30/4/003>)

View [the table of contents for this issue](#), or go to the [journal homepage](#) for more

Download details:

IP Address: 38.107.179.214

The article was downloaded on 21/02/2012 at 10:44

Please note that [terms and conditions apply](#).

# Non-invasive estimation of pulsatile flow and differential pressure in an implantable rotary blood pump for heart failure patients

A H AlOmari<sup>1</sup>, A V Savkin<sup>1</sup>, D M Karantonis<sup>2</sup>, E Lim<sup>2</sup> and N H Lovell<sup>2</sup>

<sup>1</sup> School of Electrical Engineering and Telecommunications, University of New South Wales, Sydney 2052, Australia

<sup>2</sup> Graduate School of Biomedical Engineering, University of New South Wales, Sydney 2052, Australia

E-mail: [a.savkin@unsw.edu.au](mailto:a.savkin@unsw.edu.au) and [n.lovell@unsw.edu.au](mailto:n.lovell@unsw.edu.au)

Received 4 December 2008, accepted for publication 9 February 2009

Published 12 March 2009

Online at [stacks.iop.org/PM/30/371](http://stacks.iop.org/PM/30/371)

## Abstract

We propose dynamical models for pulsatile flow and head estimation in an implantable rotary blood pump. Pulsatile flow and head data were obtained using a circulatory mock loop where fluid solutions with different values of viscosities were used as a blood analogue with varying haematocrit (HCT). Noninvasive measurements of power and pump speed were used with HCT values as inputs to the flow model while the estimated flow was used with the speed as inputs to a head estimation model. Linear regression analysis between estimated and measured flows obtained from a mock loop resulted in a highly significant correlation ( $R^2 = 0.982$ ) and a mean absolute error ( $e$ ) of  $0.323 \text{ L min}^{-1}$ , while for head,  $R^2 = 0.933$  and  $e = 7.682 \text{ mmHg}$  were obtained.  $R^2 = 0.849$  and  $e = 0.584 \text{ L min}^{-1}$  were obtained when the same model derived in the mock loop was used for flow estimation in *ex vivo* porcine data ( $N = 6$ ). Furthermore, in the steady state, the solution of the presented flow model can be described by a previously designed and verified static model. The models developed herein will play a vital role in developing a robust control system of the pump flow coping with changing physiological demands.

Keywords: implantable rotary blood pumps, non-invasive pulsatile flow estimation, pressure head estimation, left ventricular assist device, heart pump differential pressure estimation

## 1. Introduction

Sensorless estimation of blood flow and differential pressure (head) for implantable rotary blood pumps (iRBPs) is crucial in designing an automatic, robust and responsive control

system that effectively controls the blood flow according to the body's physiological needs and perturbations (Wakisaka *et al* 1998, Khalil *et al* 2008, Chen *et al* 2005, Oshikawa *et al* 2000). Various groups have shown that such controllers are important to avoid and detect pumping states associated with abnormal flow conditions (Karantonis *et al* 2006, Tanaka *et al* 2005, Ohuchi *et al* 2001).

Many research groups have tackled the problem of non-invasive estimation of the flow rate and head (for example, see Bertram (2005) and the references therein). Under steady-state conditions, it has been shown that the flow rate and head can be accurately estimated (Malagutti *et al* 2007, Ayre *et al* 2000, 2003, Funakubo *et al* 2002, Kitamura *et al* 2000, Tsukiya *et al* 1997). However, due to numerous factors that need to be taken into consideration, the pulsatile flow and head estimation of iRBPs have been much less frequently studied. Such factors, for example, may include the use of characteristic curves of the pump, where these curves are sensitive to many physiological and mechanical parameters, such as changing blood viscosity, native heart interaction, mechanical friction and impeller inertia of the pump. In addition to their contribution to the nature of the dynamical estimation approach that should be followed, these factors are also important to reach a valid and stable model to estimate the instantaneous flow and head of the pump.

The tasks of instantaneous flow and head estimation were examined by Tsukiya *et al* (2001) where they employed power and pump speed to estimate the dimensionless flow rate. Also, non-invasive measurements of power and speed were used by Yoshizawa *et al* (2002) to estimate the instantaneous flow and head values using an autoregressive with exogenous inputs (ARX) model where the current and past values of power and speed were used as inputs to another ARX model to estimate a variable  $K$  which was assumed to provide information about blood viscosity fluctuations. Their method was tested *in vitro* and using animal experiments (Tanaka *et al* 2003, Ogawa *et al* 2006).

Employing six fluid solutions representing different ranges of viscosities, the pulsatile flow was accurately estimated by Karantonis *et al* (2007) using an ARX model. While this method attained high accuracy when validated using circulatory mock loop data, it was not validated using *in vivo* data. More recently, in an initial study performed by our group, we employed a dynamical modelling approach for pulsatile flow estimation; however, only results for mock loop data were presented (AlOmari *et al* 2009). Although previous studies produced acceptable results when applied to estimate the pulsatile flow and head, some of these studies have used higher order input/output system models (Yoshizawa *et al* 2002) in which they did not study the stability of the transient response of the pump flow. Others have assumed the system to be stable (Karantonis *et al* 2007).

In the present study, we used non-invasive feedback measurements of the rotational speed and power to estimate the pump flow in a pulsatile environment using a new nonlinear dynamical model. When operated under steady-state conditions, our model can provide an accurate estimate of the pump flow which agrees with that obtained from the static model developed previously in our laboratory under non-pulsatile conditions (Malagutti *et al* 2007). More precisely, the set of steady-state solutions of our dynamical flow model coincides with the set of solutions of the static equation derived in Malagutti *et al* (2007). Then, we used the estimated pulsatile flow values together with pump rotational speed to estimate the instantaneous head values.

Other practically important requirements for our dynamical models for flow and head estimation are their stability. The proposed models will allow us to accurately study and estimate the transient response and the dynamics of the pulsatile flow and head, and will be a milestone in designing an automatic and robust control system for pump flow. Furthermore, the developed models are relatively simple and elegant which makes the corresponding control

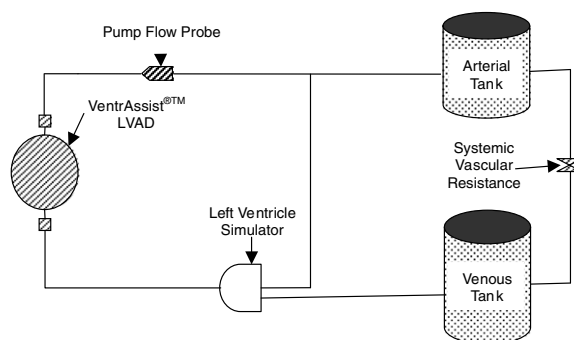


**Figure 1.** The pulsatile mock loop used to generate the experimental data for flow and head used in this study.

design problems more tractable. The pulsatile flow model was validated using an *in vitro* mock circulatory loop and *ex vivo* animal data obtained from acute implantation of a VentriAssist<sup>®</sup>™ (VentriAssist<sup>®</sup>™, Sydney, Australia) left ventricular assist device (LVAD) in healthy pigs while the head estimation model was only validated using the circulatory mock loop data.

## 2. Methods

### 2.1. Mock circulatory loop experiments

A VentriAssist<sup>®</sup>™ centrifugal iRBP was connected in a mock circulatory loop in a pulsatile environment. The mock loop was composed of venous and arterial reservoir tanks, a silicone bag which represented the left ventricular chamber, a VentriAssist<sup>®</sup>™ LVAD and suitable tubes used for connection purposes. Ventricular contraction was simulated by periodically compressing the mock ventricle with pneumatic pistons at a fixed rate. Resistances of the tubing, as well as compliances of the tanks, were set according to the human cardiovascular data available in the literature. Probes and transducers (ADInstruments, Castle Hill, NSW, Australia) were connected to the mock loop to measure different physiological signals including arterial pressure, central venous pressure, and pump inlet and outlet pressures. The pulsatile flow was measured by an ultrasonic flow probe (Transonics Systems Inc., Ithaca, NY). The schematic diagram of the pulsatile mock loop is shown in figure 1. The instantaneous rotational pump speed ( $\omega$ ), motor voltage ( $V$ ) and current ( $I$ ) were accessed as feedback signals from the pump controller. All signals were recorded using a Powerlab data acquisition system (ADInstruments, Castle Hill, NSW, Australia).

The experiments were performed using six aqueous glycerol solutions of differing viscosities to cover the range of real human blood viscosities from 2.05 to 3.56 mPas. This approximately coincides with haematocrit (HCT) values of 24, 27, 34, 39, 41 and 47.5%. To cover the entire operation range of the pump flow from  $-2$  to  $12 \text{ L min}^{-1}$  with different viscosities, the speed was varied from 1800 to 3000 rpm in a stepwise increment of 100 rpm with each step lasting for 30 s. For each step, systemic resistance was also changed to cover the range of desired flows. In agreement with the clinical situation of the majority of heart failure patients, the mock aortic valve was closed for the whole period of experimentation.

The sampling rate was 4 kHz for data recordings, but, in further analysis, the data were down-sampled to 50 Hz.

## 2.2. *Ex vivo acute pig experiments*

The VentrAssist<sup>®</sup>™ centrifugal heart pump was acutely implanted in six healthy pigs. A detailed description of the experimental protocol is provided in Ayre *et al* (2003). In each pig, the inflow pump cannula was inserted into the apex of the left ventricle while the outflow cannula was anastomosed to the ascending aorta. Indwelling catheters (DwellCath, Tuta Labs, Lane Cove, NSW, Australia) and pressure transducers (Datex-Ohmeda, Homebush, NSW, Australia) were instrumented to the pig's native heart to measure the left ventricle, left atrial, aortic and pump inlet pressures. Pump and aortic flows were measured by ultrasonic flow probes (Transonics Systems Inc., Ithaca, NY). Measurements of the pump flow and inlet pressure were obtained from a point very close to the pump input and output and not at the distal ends of the pump cannulae. Besides these signals, the non-invasive pump impeller rotational speed ( $\omega$ ), motor current ( $I$ ) and supply voltage ( $V$ ) were acquired and recorded from the pump controller. The speed control algorithm was directly programmed into the controller microprocessor. Via firmware on a hardware commutation board, the speed controller adjusts the pump speed based on speed measurements only. The speed controller does not have measurements of other variables from our model. Therefore, there is no feedback between our input and output variables. In the dynamical model presented in our paper we use speed as an input to the system, and this input does not depend on other inputs or outputs of the model. Different set points of the pump impeller rotational speed were used to test the pump performance at different physiologically significant pumping states including ventricular collapse (VC) and aortic valve not opening (ANO). All the aforementioned signals were recorded using a Powerlab data acquisition system (ADInstruments, Castle Hill, NSW, Australia). The experimental data were sampled at 200 Hz. For a more detailed description of the experimental data acquisition, see Karantonis *et al* (2006).

## 2.3. *Dynamical modelling*

**2.3.1. Pulsatile flow.** A non-invasive, steady-state average flow ( $Q_{ss}$ ) estimator was designed in a non-pulsatile environment for the iRBP. The flow estimator was based on the input power ( $P$ ) and rotational speed ( $\omega$ ). The static equation for the flow estimator is based on the work of Malagutti *et al* (2007) and Ayre *et al* (2003) and is of the following form:

$$Q_{ss} = a + bP + cP^2 + dP^3 + e\omega + h\omega^2, \quad (1)$$

where  $P = VI$  is the product of supply voltage ( $V$ ) and motor current ( $I$ ),  $a$ ,  $e$ , and  $h$ , are constants and the power coefficients  $b$ ,  $c$ , and  $d$  were described as having linear relationships with HCT (Malagutti *et al* 2007).

Now, we describe a dynamical flow model for the iRBP. The main requirement for the dynamical model is that any steady-state solution of the dynamical model be a solution of the static equation (1). Furthermore, any steady-state solution of the dynamical model should be stable. We introduce a variable  $f(k)$  as follows:

$$f(k) = g(P(k), \omega(k)), \quad (2)$$

where

$$g(P(k), \omega(k)) = a + bP(k) + cP^2(k) + dP^3(k) + e\omega(k) + h\omega^2(k). \quad (3)$$

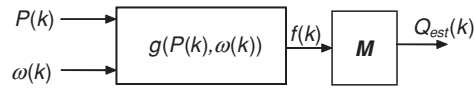


**Figure 2.** The input/output block diagram for the dynamical system model  $\mathbf{M}$  used to estimate the pulsatile flow  $Q(k)$ .

Here,  $k$  is the discrete time satisfying  $t = kh$  and  $h > 0$  is the sampling interval. In other words, the variable  $f(k)$  represents the right-hand side of the static equation (1), describing the pump flow in a steady state. We introduce a dynamical model ( $\mathbf{M}$ ) of the form

$$(A(\nabla) + B(\nabla))Q_{\text{est}}(k) = B(\nabla)f(k), \tag{4}$$

where  $Q_{\text{est}}(k)$  is the output of the system which represents the estimated instantaneous values of the pulsatile flow  $Q(k)$ ,  $f(k)$  is the input to the dynamical system model  $\mathbf{M}$ ,  $\nabla$  is the discrete time backward shift operator, and  $A(\nabla)$  and  $B(\nabla)$  are polynomials defined as follows:

$$A(\nabla)Q_{\text{est}}(k) = \sum_{i=0}^n a_i Q_{\text{est}}(k - i + 1), \tag{5}$$

$$B(\nabla)f(k) = \sum_{j=1}^m b_j f(k - j + 1). \tag{6}$$

Here,  $n$  is the model output order and  $m$  is the model input order satisfying the condition  $m \leq n$ . We assume that  $A(1) = 0$  and  $B(1) \neq 0$ . This yields the following conditions on the parameter coefficients of the model:

$$\sum_{i=0}^n a_i = 0, \tag{7}$$

$$\sum_{j=1}^m b_j \neq 0. \tag{8}$$

The block diagram of the system with a dynamical model  $\mathbf{M}$  is illustrated in figure 2.

Now we describe all steady-state or constant solutions of equation (3). Let  $Q_{\text{est}}(k) \equiv Q_0$  and  $f(k) \equiv f_0$  for all  $k = 0, 1, 2, 3, \dots$ ; then, we obtain from (4) that

$$(A(1) + B(1))Q_0 = B(1)f_0. \tag{9}$$

Under the assumptions (7) and (8), it immediately follows from (9) that

$$Q_0 = f_0. \tag{10}$$

Since  $f(k)$  is defined by (2), (3) and (10), it implies that  $Q_0$  is the corresponding solution of equation (1). In other words, under the assumptions (7) and (8), the set of steady states of our dynamical model (4) coincides with the set of solutions of equation (1). Hence, steady states of the dynamical model are described by the static model. Furthermore, if  $(A(\nabla) + B(\nabla))$  is stable, i.e. all poles of the system are inside the unit disk (Ogata 1995), then the solution of the dynamical system (4) with any initial conditions and with a constant input  $f_0$  will converge to the constant output  $Q_0$  satisfying (10). Furthermore, the stability of the model means that for any bounded input  $f(k)$ , a bounded flow output  $Q_{\text{est}}(k)$  will result.

2.3.2. *Head.* We used an ARX model to derive a stable model for head estimation using as inputs the estimated pulsatile flow values and rotational speed. A discrete time ARX model with two input signals can be described as follows (Ljung 1999):

$$C(\nabla)H_{\text{est}}(k) = D_1(\nabla)Q_{\text{est}}(k) + D_2(\nabla)\omega(k), \quad (11)$$

where

$$C(\nabla) = 1 + c_1\nabla^{-1} + c_2\nabla^{-2} + \dots + c_n\nabla^{-n}, \quad (12)$$

$$D_1(\nabla) = d_{11}\nabla^{-1} + d_{12}\nabla^{-2} + \dots + d_{1m}\nabla^{-m} \quad (13)$$

and

$$D_2(\nabla) = d_{21}\nabla^{-1} + d_{22}\nabla^{-2} + \dots + d_{2m}\nabla^{-m}. \quad (14)$$

Here  $H_{\text{est}}(k)$  is the estimated head,  $Q_{\text{est}}(k)$  is the estimated pulsatile flow,  $\omega(k)$  is the impeller rotational speed of the pump,  $n$  is the model output order and  $m$  is the input model order. The resulting proposed model for the head estimation of the pump was not validated using the animal experiments because we did not have accurate measurement of pump outflow pressure. Therefore, the head estimation model was validated using the mock circulatory loop data only.

2.3.3. *System identification and data analysis.* The mock loop data were divided into two sets: one set was used for system identification while the other was used along with the animal data ( $N = 6$ ) to validate those models. The first set of data consisted of three experiments corresponding to the solution viscosities of 2.05, 2.66 and 3.26 mPas, while the other set contained data from the other three experiments with viscosities of 2.35, 2.95 and 3.56 mPas together with all the animal experimental data. In both, identification and validation data sets, the changes in the pump target speed were included in the data so that the transient response of the pump flow and head could be identified. In the system identification process, an off-line-restricted least-squares method was used to estimate the parameter coefficients of the pulsatile flow model while a least-squares method (Ljung 1999) was used to estimate coefficients for the head estimation model. Values of parameter coefficients of the pulsatile flow estimation model were chosen so that the error between estimated  $Q_{\text{est}}(k)$  and measured flows  $Q_{\text{meas}}(k)$  was minimized. Simultaneously, however, the resulting flow model parameter coefficients should fulfil the assumptions previously defined in equations (7) and (8).

Similarly, in the head modelling, we divided the head data into two sets: one was used for system identification while the other set was used to generate  $Q_{\text{est}}(k)$  using the derived flow estimation model and this was used with the corresponding values of the rotational speed  $\omega(k)$  as inputs to the head model to estimate instantaneous values of  $H_{\text{est}}(k)$ . Also, parameter coefficients of the head estimation model were selected to minimize the error between the estimated ( $H_{\text{est}}(k)$ ) and measured heads ( $H_{\text{meas}}(k)$ ). The function *arx* in the System Identification Toolbox of MATLAB R2007b<sup>®</sup> (The Mathworks, Inc., Natick, MA) was used to identify the coefficients of the ARX model described in equations (12)–(14).

In both cases, the model output order ( $n$ ) and the input order ( $m$ ) were varied from 1 to 10 and the delay value was determined by estimating the impulse response of the system by cross-correlation analysis between the input ( $s$ ) and output signals, with a value of 1 being used for both flow and head estimation models. The delay value was also set to a value of 1 when the pulsatile flow estimation model was used to estimate the flow in the animal experiments. The mean absolute error ( $e$ ) and correlation coefficient ( $R$ ) between  $Q_{\text{est}}$ ,  $Q_{\text{meas}}$  and  $H_{\text{est}}$ ,  $H_{\text{meas}}$  were used to check the performance and to evaluate the estimation accuracy of the models. Values of  $e$  and  $R$  were evaluated as follows:

**Table 1.** Values of the parameter coefficients for the system model shown in equation (17).

Coefficient	Value
$a_0$	1.0000
$a_1$	-2.2562
$a_2$	1.4950
$a_3$	-0.2397
$b_1$	0.2710
$b_2$	-0.2546

$$e = \frac{1}{N} \sum_{i=1}^N (y_{\text{meas}}(k) - y_{\text{est}}(k))^2, \quad (15)$$

$$R = \frac{\sum_{i=1}^N (y_{\text{meas}}(k) - \overline{y_{\text{meas}}})(y_{\text{est}}(k) - \overline{y_{\text{est}}})}{(\sum_{i=1}^N (y_{\text{meas}}(k) - \overline{y_{\text{meas}}})^2 \sum_{i=1}^N (y_{\text{est}}(k) - \overline{y_{\text{est}}})^2)^{1/2}}. \quad (16)$$

Here,  $N$  is the length of data.  $\overline{y_{\text{meas}}}$  and  $\overline{y_{\text{est}}}$  are the mean values of the measured and estimated pulsatile flows or head, respectively.

The results obtained when using either of the two sets of data for identification and the other for validation attained the same degree of accuracy for both the pulsatile flow and head estimation tasks. To reduce the contributions of external sources in the identification process of the systems, all sets of data were explicitly pre-treated to remove trends and offsets by direct subtraction. All simulations, linear regression analysis, model implementation and algorithms were performed in MATLAB R2007b<sup>®</sup> (The Mathworks, Inc., Natick, MA). The models were implemented on a PC running Windows XP.

### 3. Results

#### 3.1. Mock loop

**3.1.1. Pulsatile flow.** The model output for the pulsatile flow was checked according to the performance of  $e$  and  $R$  for different combinations of  $m$  and  $n$ . The best results were obtained with system model orders of  $n = 3$ ,  $m = 2$  and delay value = 1. This combination gave the least mean absolute error ( $e$ ) and highest correlation coefficient ( $R$ ) between the estimated and measured flows and satisfied the conditions in equations (7) and (8). The resulting system model is described by the following difference equation:

$$\begin{aligned} a_0 Q_{\text{est}}(k+1) + (a_1 + b_1) Q_{\text{est}}(k) + (a_2 + b_2) Q_{\text{est}}(k-1) + a_3 Q_{\text{est}}(k-2) \\ = b_1 f(k) + b_2 f(k-1), \end{aligned} \quad (17)$$

where  $Q_{\text{est}}(k)$  is the estimated pulsatile flow and  $f(k)$  is the input signal. The parameter coefficients of the system are shown in table 1. The poles–zeros plot of the system model shown in figure 3 demonstrates that all poles are inside the unit circle, satisfying the stability of the model criteria. The dominant pole and a zero are close in value but are not exactly the same; there is a 5% difference in the absolute value between them. The reduced order model gave a high and clinically unacceptable mean absolute error ( $e$ ) with a low correlation coefficient ( $R$ ) between estimated and measured pulsatile flows in both mock loop and animal experiments.

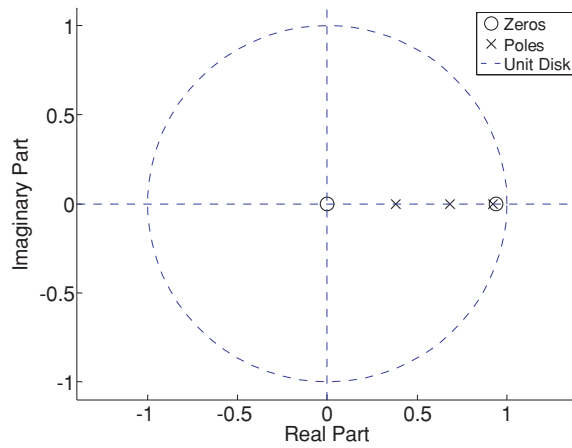


**Figure 3.** Poles–zeros plot of the system model described in equation (17). The system is stable as all poles are inside the unit circle.

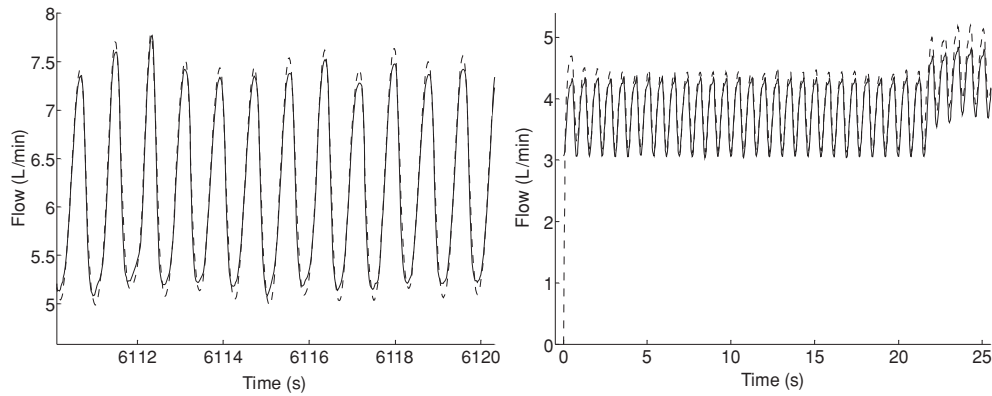


**Figure 4.** Estimated pulsatile flow compared with the measured flow obtained from mock loop experiments at  $\omega = 2800$  rpm and HCT = 27% (equivalent to a viscosity value of 2.35 mPas) (left panel). The transient response of the pulsatile flow estimation model described in equation (17) from initial conditions to a steady state and also the model response for target speed changes from  $\omega = 1800$  rpm to 2000 rpm with HCT = 37% (equivalent to a viscosity value of 2.95 mPas) at time 21.6 s (right panel). The solid line is the measured flow ( $Q_{\text{meas}}$ ), while the dashed line shows the estimated flow ( $Q_{\text{est}}$ ).

The dashed line in figure 4 (left and right panels) shows part of the estimated pulsatile and recorded measured flows together with the transient response of the pulsatile flow estimation model obtained from one of the mock loop experiments. Linear regression analysis between  $Q_{\text{est}}(k)$  and  $Q_{\text{meas}}(k)$  obtained from the circulatory pulsatile mock loop experiments for 27% HCT, 37% and 47.5% of aqueous glycerol solutions is illustrated in figures 5(a)–(c). Values of the correlation coefficient ( $R^2$ ) and slope of the linear regression line ( $l$ ), in addition to the mean absolute error value ( $e$ ), were obtained from each pulsatile mock loop experiment. Analysing all mock loop data in the validation set resulted in a highly significant correlation ( $R^2 = 0.982$ ) between estimated and measured with a small mean absolute error value ( $e = 0.323 \text{ L min}^{-1}$ ). The mean slope of the linear regression line was very close to unity (0.978).

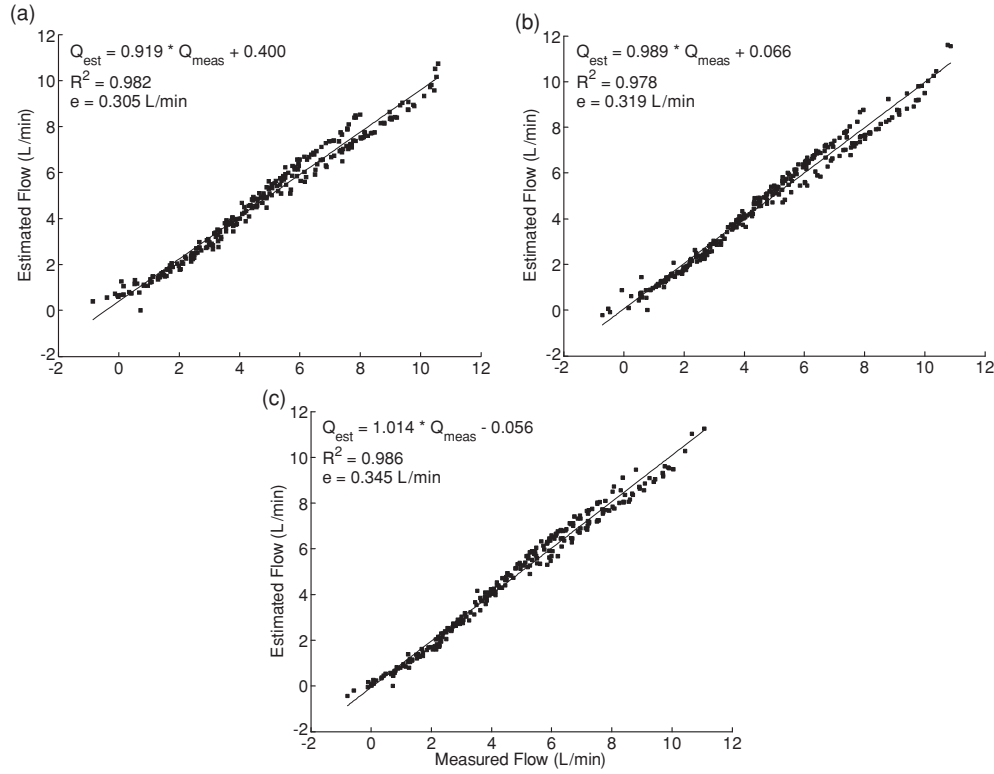


**Figure 5.** Linear regression plot between estimated versus measured flows obtained from a circulatory pulsatile mock loop for (a) HCT = 27% (equivalent to 2.35 mPas viscosity), (b) HCT = 37% (equivalent to 2.95 mPas viscosity) and (c) HCT = 47.5% (equivalent to 3.56 mPas viscosity). The resulting slopes of linear regression lines are  $l = 0.919, 0.989$  and  $1.014$ , respectively.

**3.1.2. Head.** The head estimation model with  $n = 2$ ,  $m = 4$  and delay value = 1 that produced the highest correlation coefficient ( $R$ ) and least mean absolute error ( $e$ ) between  $H_{\text{est}}(k)$  and  $H_{\text{meas}}(k)$  is defined as follows:

$$C(\nabla)H_{\text{est}}(k) = D_1(\nabla)Q_{\text{est}}(k) + D_2(\nabla)\omega(k) + \lambda, \quad (18)$$

where

$$C(\nabla) = 1 - 1.735\nabla^{-1} + 0.758\nabla^{-2}, \quad (19)$$

$$D_1(\nabla) = -1.157\nabla^{-1} + 1.519\nabla^{-2} - 0.278\nabla^{-3} - 0.475\nabla^{-4}, \quad (20)$$

$$D_2(\nabla) = 0.0683\nabla^{-1} - 0.0742\nabla^{-2} - 0.0298\nabla^{-3} + 0.0379\nabla^{-4}. \quad (21)$$

Here  $H_{\text{est}}(k)$  is the estimated instantaneous head,  $Q_{\text{est}}(k)$  is the estimated pulsatile flow,  $\omega(k)$  is the instantaneous rotational speed,  $\lambda = -0.476$  is a constant value and  $\nabla$  is the discrete time backward shift operator. Figures 6(a) and (b) show the poles and transmission zeros plot of the head estimation system. It is noticeable that the proposed model is stable as all poles are inside the unit circle. As the value of delay between input (s) and output signals increased, the pulsatile flow and head estimation models became unstable. It should be pointed out that unlike our pump flow model (17), the proposed equation (18) for head estimation has the

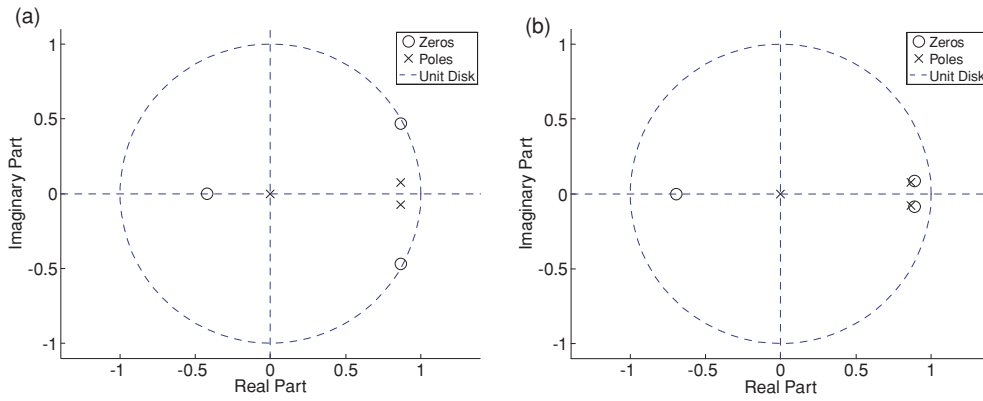


**Figure 6.** Poles and transmission zeros plot of the head estimation ( $H_{est}$ ) model from (a)  $Q_{est}(k)$  and (b)  $\omega(k)$ .

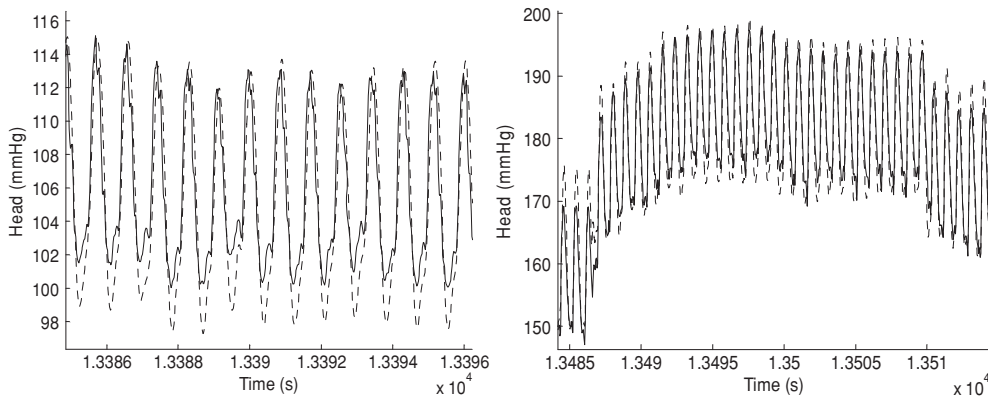


**Figure 7.** Estimated head ( $H_{est}$ ) compared with the measured head ( $H_{meas}$ ) obtained from a mock loop at  $\omega = 2400$  rpm and an HCT of 37% equivalent to a viscosity value of 2.95 mPas (left panel). The transient response of the head estimation model to target speed changes from  $\omega = 2900$  rpm to 3000 rpm at time 13 486 s and from  $\omega = 3000$  rpm back to 2900 rpm at time 13 509 s with HCT = 27% (equivalent to a viscosity value of 2.35 mPas) (right panel). The solid line is the measured head ( $H_{meas}$ ), while the dashed line shows the estimated head ( $H_{est}$ ).

constant term  $\lambda$  which makes this model nonlinear. There is a 5% difference in the absolute value between poles and transmission zeros shown in figure 6(b). Model reduction was not possible here because of the constant value  $\lambda$  in the system model in equation (18). Figure 7 shows the comparison between the estimated and measured head together with the transient response of the head estimation model in one of the mock loop experiments. Linear regression analysis between  $H_{est}$  and  $H_{meas}$  using mock loop data is shown in figures 8(a)–(c). Overall, a mean absolute error ( $e = 7.682$  mmHg) and a highly significant correlation ( $R^2 = 0.933$ ) were obtained.

### 3.2. Animal experiments

During animal experimentation, the values of HCT were not measured. Instead, for each animal we used the values of HCT that gave the best fit between the estimated and

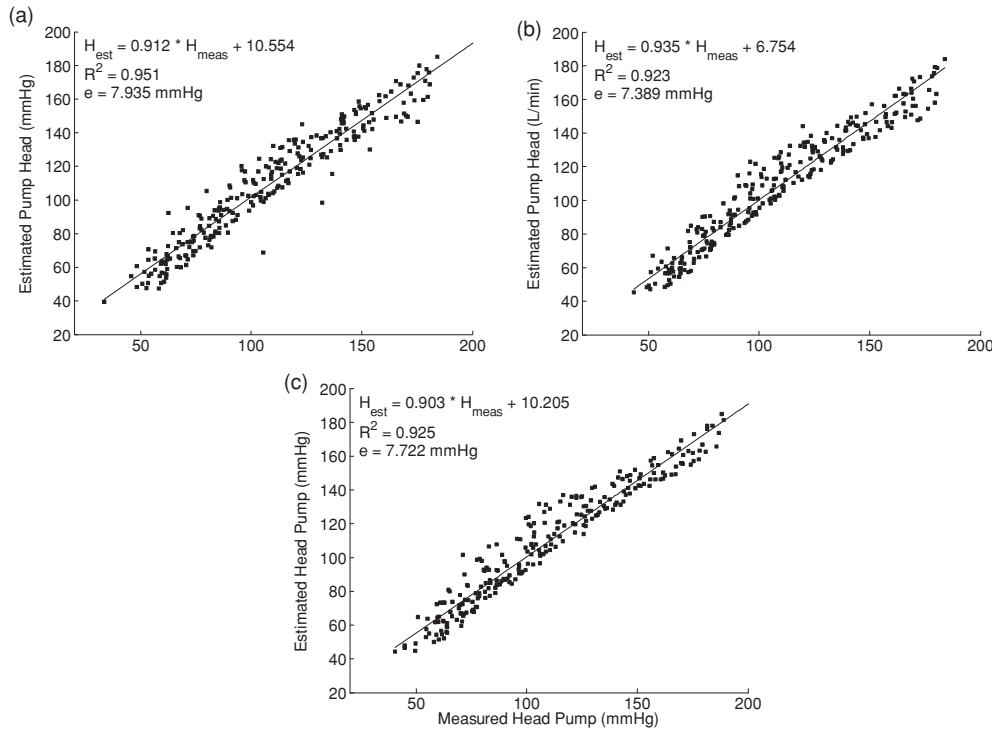


**Figure 8.** Linear regression plot between the estimated versus the measured pressure head obtained from the circulatory pulsatile mock loop for (a) 27% of HCT, (b) 37% and (c) 47.5%. The resulting slopes of linear regression lines are  $l = 0.912$ ,  $0.935$  and  $0.903$ , respectively.

**Table 2.** Linear regression analysis results between estimated and measured flows from six acute pig experiments. Results for all animals show mean  $\pm$  sem where appropriate.

Experiment	Parameter				
	$R^2$	$l$	$\alpha$	Flow range (min–max) ( $L \min^{-1}$ )	$e$ ( $L \min^{-1}$ )
Pig 1	0.897	0.951	0.269	–0.5–7	0.324
Pig 2	0.855	0.872	0.515	–0.7–7	0.343
Pig 3	0.691	0.883	0.395	–3.5–8	1.193
Pig 4	0.935	0.953	–0.056	–0.7–7	0.299
Pig 5	0.794	0.891	0.532	–2.5–8	1.043
Pig 6	0.921	0.974	0.696	–0.5–7	0.302
All animals	$0.849 \pm 0.038$	$0.921 \pm 0.018$	$0.391 \pm 0.107$	–3.5–8	$0.584 \pm 0.170$

measured flows in the steady-state model described in equation (1). The comparison between estimated pulsatile and measured flows together with the transient response of the pulsatile flow estimation model described in equation (17) in one animal experiment is shown in figure 9. Figure 10 illustrates the linear regression analysis between  $Q_{est}(k)$  and  $Q_{meas}(k)$  obtained from animals ( $N = 6$ ). The correlation coefficient ( $R^2$ ), slope of the linear regression line ( $l$ ) and offset value ( $\alpha$ ) are shown in table 2 for each animal. The correlation between estimated and measured flows was  $R^2 = 0.849$ , with a small mean absolute error ( $e = 0.584 L \min^{-1}$ ).

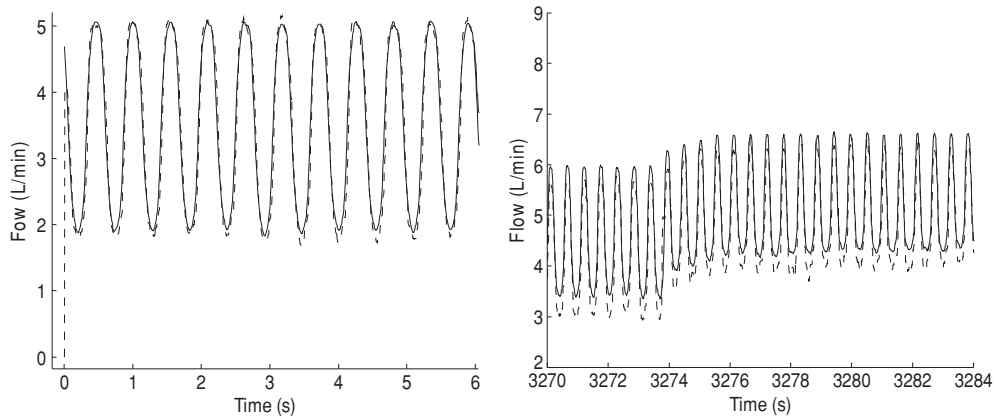


**Figure 9.** Estimated pulsatile flow ( $Q_{est}$ ) compared with the measured flow ( $Q_{meas}$ ) in one animal experiment at  $\omega = 1800$  rpm (left panel). The transient response of the pulsatile flow estimation model to the target speed changes from  $\omega = 1900$  to  $2000$  rpm at time  $3273.5$  s in one of the animal experiments (right panel). The solid line is the measured flow ( $Q_{meas}$ ), while the dashed line shows the estimated pulsatile flow ( $Q_{est}$ ).

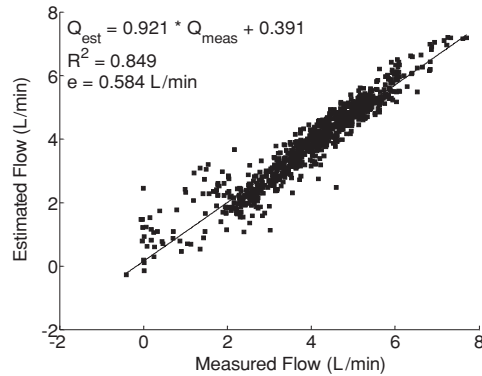


**Figure 10.** Linear regression plot between estimated ( $Q_{est}$ ) versus measured ( $Q_{meas}$ ) flows obtained from animal data ( $N = 6$ ).

The smaller correlation in two data sets (pig 3 and pig 5) and a relatively high error between estimated and measured flows were due to the excessively noisy nature of the power signals in these data sets where they do not continue to follow the fluctuations of the low and high flow ranges; rather, they intermittently reach minimum and maximum plateau values. The model can provide an accurate estimate for the negative flow up to  $-0.7 \text{ L min}^{-1}$  as shown in figure 11. Figure 11 shows the pulsatile flow estimation model response in the negative flow region, where the power signal becomes increasingly noisy.

The responses of the proposed model to abnormal flow conditions associated with different pumping states such as VC and ANO are shown in figures 12 and 13 respectively. As shown, the model accurately predicts the flow during these two states.

#### 4. Discussion

In the present study, dynamical models for pulsatile flow and head estimation were successfully designed and validated. The pulsatile flow model used as inputs the noninvasive measurements

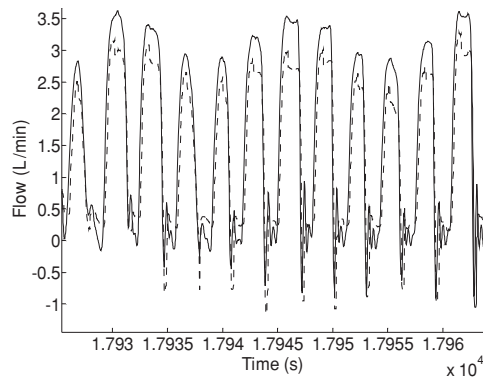


**Figure 11.** Estimated and measured flows in a negative region up to  $-1 \text{ L min}^{-1}$  with  $\omega = 1800 \text{ rpm}$  in one of the animal experiments. The solid line is the measured flow, while the dashed line shows the estimated pulsatile flow. Note that the model is able to accurately estimate the pulsatile flow in negative regions up to  $-0.7 \text{ L min}^{-1}$ .

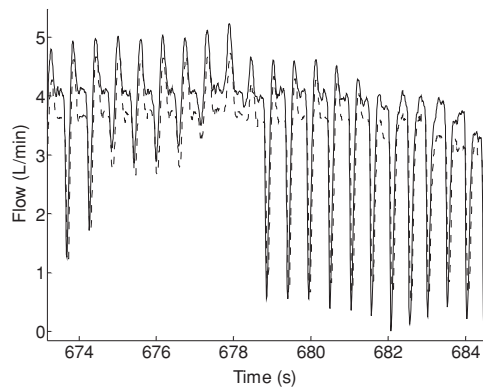


**Figure 12.** Estimated and measured flows associated with intermittent ventricular collapse in animal data. The solid line is the measured flow ( $Q_{\text{meas}}$ ), while the dashed line shows the estimated pulsatile flow ( $Q_{\text{est}}$ ). Note that the deep peaks were accurately estimated.

of power and speed, while the estimated instantaneous values of the pulsatile flow together with the rotational speed were used as inputs to the head estimation model. The models developed in our paper were only pump models and not pump and cannulae models, and there are no parameters in the models which relate to the cannulae, so the dimensions of the cannulae should not affect the results obtained in our paper because the data for the pump pulsatile flow and inlet pressure were obtained very close to the pump input and output and not at the ends of the pump cannulae.

At the time of animal experimentation, HCT was not routinely measured as it was not believed to vary significantly in stable, anaesthetised animal preparations. Moreover, the impact of HCT on the flow estimation was not believed to be significant. While the former observation is true, the latter was subsequently found to be incorrect. In the proposed models, the level of HCT was assumed to be known. This is a major limitation of clinical utility of the present models. Further research of online estimation of HCT is being conducted in our laboratory. It should be noted that, in a VentrAssist LVAD, HCT fluctuations are highly correlated with the power coefficients which play a major role in the static flow estimator

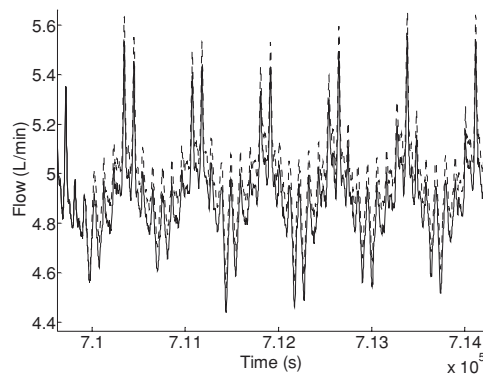


**Figure 13.** Estimated and measured flows associated with the intermittent aortic valve not opening pumping state. The solid line is the measured flow ( $Q_{\text{meas}}$ ), while the dashed line shows the estimated pulsatile flow ( $Q_{\text{est}}$ ).

equation derived in Malagutti *et al* (2007) and used to build the dynamical model in this paper (equation (1)).

Results obtained by Tsukiya *et al* (2001) showed that their non-pulsatile flow rate estimation method was able to monitor the instantaneous values of flow. A  $1 \text{ L min}^{-1}$  mean flow rate error was obtained. In addition to data obtained from chronic and acute sheep flow experiments, Ayre *et al* (2003) have used static, non-pulsatile and pulsatile mock loops with aqueous glycerol solutions and ovine blood to derive average flow estimation algorithms. Their results produced high values of  $R^2$  for *in vitro* (0.997) and *in vivo* (0.986) experiments. On the other hand, using an ARX model, Yoshizawa *et al* (2002) developed an instantaneous flow and head estimator for a mock loop. For flow estimation, a mean absolute error of  $1.66 \text{ L min}^{-1}$  and a correlation coefficient of 0.85 were reported, while for pressure, a mean absolute error of 12.8 mmHg and a correlation coefficient of 0.906 were obtained.

Tanaka *et al* (2003) performed *in vivo* tests to validate the method proposed by Yoshizawa *et al* (2002). They obtained an estimation error of  $0.27 \text{ L min}^{-1}$  and a correlation coefficient of 0.875 for flow, as well as an estimation error of 6.77 mmHg and a correlation coefficient of 0.775 for pressure. In a related study by Ogawa *et al* (2006), a single chronic animal experiment was conducted to evaluate the flow estimation method proposed by Yoshizawa *et al* (2002). In their study, a mean square error of  $0.80 \text{ L min}^{-1}$  and a correlation coefficient of 0.964 were obtained. More recently, the pulsatile flow was accurately estimated in a mock loop by Karantonis *et al* (2007) using different formulations of an ARX model.

In comparison with the aforementioned studies, the models proposed in this paper produced superior results in the mock loop setting. For pulsatile flow estimation, it resulted in a high correlation coefficient  $R^2 = 0.982$  with a mean absolute error  $e = 0.323 \text{ L min}^{-1}$  while for head,  $R^2 = 0.933$  and  $e = 7.682 \text{ mmHg}$  were obtained. The pulsatile flow estimation model was also validated using *ex vivo* animal data ( $N = 6$ ) which resulted in  $R^2 = 0.849$  and  $e = 0.584 \text{ L min}^{-1}$ , which is comparable with previous results obtained from animal experiments. Furthermore, the proposed pulsatile and head estimation models are inherently stable allowing us to easily and accurately study the transient responses.

Deviations between estimated and measured pulsatile flows were noticed at low and high flows. This may be due to the linear relation assumed between the function  $f(k)$  derived from the static flow estimator described in equation (1) and the output pulsatile flow represented by the dynamical model described in equation (4). Another reason may be the effects of a higher

percentage error in the flow probe reading at low flow rates. In the mock loop, eddy currents and undetected air bubbles may affect measurements at high flow rates (Malagutti *et al* 2007).

In this study, for the first time, we employ the steady-state model in a pointwise manner to obtain a low order dynamical model to estimate the pulsatile flow. Also, the rotational speed values and estimated pulsatile flow are used as inputs to another dynamical model to estimate the pump head in the pulsatile environment. Furthermore, we studied the stability of the transient responses of the proposed models. This will facilitate the use of these models in future work and simplify the design of a control system for closed loop control of the pump.

## 5. Conclusion and future research

Two stable dynamical models were proposed for pulsatile flow and head estimation in an iRBP. In the flow estimation model, the non-invasive measurements of power and rotational speed were used as inputs. Furthermore, the proposed flow estimation model is stable and its set of steady states is identical to the set of solutions of the previously derived static model. Future research will include the combination of the presented models with a cardiovascular model developed in our laboratory by Lim *et al* (2007). This will help in understanding the response of the models to actual perturbations and changes in physiological parameters. Also, this combination will help in the design of future control algorithms.

## Acknowledgment

This work was supported in part by the Australian Research Council.

## References

- AlOmari A H, Savkin A V, Karantonis D M, Lim E and Lovell N H 2009 A dynamical model for pulsatile flow estimation in a left ventricular assist device *BIOSIGNALS: Proc. of 2nd Int. Conf. on Bio-inspired Systems and Signal Processing (Porto, Portugal)* vol 2, pp 402–5
- Ayre P J, Lovell N H and Woodard J C 2003 Non-invasive flow estimation in an implantable rotary blood pump: a study considering non-pulsatile and pulsatile flow *Physiol. Meas.* **24** 179–98
- Ayre P J, Vidakovic S S, Tansley G D, Watterson P A and Lovell N H 2000 Sensorless flow and head estimation in the VentrAssist rotary blood pump *Artif. Organs* **24** 585–8
- Bertram C D 2005 Measurement for implantable rotary blood pumps *Physiol. Meas.* **26** R99–117
- Chen S, Antaki J F, Simaan M A and Boston J R 2005 Physiological control of left ventricle assist devices based on gradient of flow *Proc. 2005 American Control Conf.* vol 6 pp 3829–34
- Funakubo A, Ahmed S, Sakuma I and Fukui Y 2002 Flow rate and pressure head estimation in a centrifugal blood pump *Artif. Organs* **26** 985–90
- Karantonis D M, Cloherty S L, Mason D G, Ayre P J and Lovell N H 2007 Noninvasive pulsatile flow estimation for an implantable rotary blood pump *Proc. of the 29th Ann. Int. Conf. of the IEEE Eng. Med. Biol. Soc.* pp 1018–21
- Karantonis D M, Lovell N H, Ayre P J, Mason D G and Cloherty S L 2006 Identification and classification of the physiologically significant pumping states in an implantable rotary blood pump *Artif. Organs* **30** 671–9
- Khalil H A, Kerr D T, Franchek M A, Metcalfe R W, Benkowski R J, Cohen W E, Tuzun E, Radovancevic B, Frazier O H and Kadipasaoglu K A 2008 Continuous flow total artificial heart: modeling and feedback control in a mock circulatory system *ASAIO J.* **54** 249–55
- Kitamura T, Matsushima Y, Tokuyama T, Kono S, Nishimura K, Komeda M, Yanai M, Kijima T and Nojiri C 2000 Physical model-based indirect measurements of blood pressure and flow using a centrifugal pump *Artif. Organs* **24** 589–93
- Lim E, Cloherty S L, Reizes J A, Mason D G, Salamonsen R F, Karantonis D M and Lovell N H 2007 A dynamic lumped parameter model of the left ventricular assisted circulation *Proc. of the 29th Ann. Int. Conf. of the IEEE Eng. Med. Biol. Soc.* pp 3990–3
- Ljung L 1999 *System Identification: Theory for the User* 2nd edn (Englewood Cliffs, NJ: Prentice-Hall)

- Malagutti N, Karantonis D M, Cloherty S L, Ayre P J, Mason D G, Salamonsen R F and Lovell N H 2007 Noninvasive average flow estimation for an implantable rotary blood pump: a new algorithm incorporating the role of blood viscosity *Artif. Organs* **31** 45–52
- Ogata K 1995 *Discrete-Time Control Systems* 2nd edn (Englewood Cliffs, NJ: Prentice-Hall)
- Ogawa D *et al* 2006 Indirect flow rate estimation of the NEDO PI Gyro pump for chronic BVAD experiments *ASAIO J.* **52** 266–71
- Ohuchi K, Kikugawa D, Takahashi K, Uemura M, Nakamura M, Murakami T, Sakamoto T and Takatani S 2001 Control strategy for rotary blood pumps *Artif. Organs* **25** 366–70
- Oshikawa M, Araki K, Endo G, Anai H and Sato M 2000 Sensorless controlling method for a continuous flow left ventricular assist device *Artif. Organs* **24** 600–5
- Tanaka A, Yoshizawa M, Abe K, Takeda H, Yambe T and Nitta S 2003 *In vivo* test of pressure head and flow rate estimation in a continuous-flow artificial heart *Artif. Organs* **27** 99–103
- Tanaka A, Yoshizawa M, Olegario P, Ogawa D, Abe K, Motomura T, Igo S and Nosé Y 2005 Detection and avoiding ventricular suction of ventricular assist devices *Proc. of the 2005 IEEE Engineering in Medicine and Biology 27th Ann. Conf.* pp 402–5
- Tsukiya T, Akamatsu T, Nishimura K, Yamada T and Nakazeki T 1997 Use of motor current in flow rate measurement for the magnetically suspended centrifugal blood pump *Artif. Organs* **25** 692–6
- Tsukiya T, Taenaka Y, Nishinaka T, Oshikawa M, Ohnishi H, Tatsumi E, Takano H, Konishi Y, Ito K and Shimada M 2001 Application of indirect flow rate measurement using motor driving signals to a centrifugal blood pump with an integrated motor *Artif. Organs* **25** 692–6
- Wakisaka Y, Okuzono Y, Taenaka Y, Chikanari K, Endo S, Masuzawa T and Takano H 1998 Development of a flow estimation and control system of an implantable centrifugal blood pump for circulatory assist *Artif. Organs* **22** 488–92
- Yoshizawa M, Sato T, Tanaka A, Abe K, Takeda H, Yambe T, Nitta S and Nose Y 2002 Sensorless estimation of pressure head and flow of a continuous flow artificial heart based on input power and rotational speed *ASAIO J.* **48** 443–8